Low Temperature Solution Processed Transparent QLED Using Inorganic Metal Oxide Carrier Transport Layers

Yang Yu, You Liang, Jason Yong, TianZhi Li, Md Sharafat Hossain, Yutong Liu, Yihong Hu, Kumaravelu Ganesan, Efstratios Skafidas**

Y. Yu, Dr. Y. Liang, Dr. J. Yong, T. Li, Dr. M. S. Hossain, Y. Liu, Prof. E. Skafidas
Department of Electrical and Electronic Engineering, The University of Melbourne, VIC 3010, Australia. (Email: yyu5@student.unimelb.edu.au, sskaf@unimelb.edu.au)

Y. Hu
School of Engineering, RMIT University, Melbourne, VIC 3010, Australia.

Keywords: quantum dots, light emitting diodes, low temperature solution processes, transparent electronics

Abstract

Quantum dot light emitting diodes (QLEDs) are exciting new technology that have many desirable attributes when compared to existing organic LEDs (OLEDs) including increased brightness, contrast and response time. Solution based fabrication approaches have the advantage of being able to produce large area electronic systems at reduced costs and critical in applications such as large display fabrication and electronics on curved surfaces including low-profile augmented reality glasses. In this paper, we, for the first time, describe a fully solution processed transparent inorganic QLED. Traditional QLED fabrication methodologies require the use of air-sensitive materials that make fabrication of these devices challenging and expensive. Instead of using air-sensitive organic materials, in our approach, nickel oxide (NiO) is used as the hole transport layer and is deposited using a sol-gel method. We investigate copper doping of the NiO to reduce the turn-on voltage of the QLED device. Importantly, the post-annealing temperature of the sol-gel process is below 275 ℃ which permits the fabrication of QLEDs on a wide range of substrates. Our experimental results are

This is the author manuscript accepted for publication and has undergone full peer review but has not been through the copyediting, typesetting, pagination and proofreading process, which may lead to differences between this version and the Version of Record. Please cite this article as doi: 10.1002/adfm.202106387.

concordant with the COMSOL simulation data and demonstrate the feasibility of fabricating fully transparent inorganic QLED devices using a solution-based process.

1. Introduction:

During the past decade, organic light emitting diode (OLED) displays have gradually replaced traditional liquid crystal displays (LCD). A promising emission layer material for LEDs is inorganic colloidal quantum dots (QDs) and they have been attracting growing research interest.[1–3] Compared to the well-known organic emission layer materials, QDs, which are excellent candidates for next generation displays, possess many advantages including: tuneable wavelength, purer colour, longer lifetime, higher brightness and are compatible with solution process. [4–6]

A great amount of effort has been devoted towards the realization of transparent flexible electronics. Various manufacturing processes have been demonstrated, including sputtering, e-beam evaporation and solution processes.[7–10] Among them, solution processes have the advantage of low-temperature and do not require vacuum[11,12]. It has also been reported that inorganic wide bandgap transparent semiconductive thin films, such as metal oxide, can be synthesised via a sol-gel solution process. [13–15] These thin films are produced by deposition undertaken by either printing or spin-coating and followed by post-annealing. With the addition of suitable fuels to the ink mixture, the post-annealing temperature can be reduced by a novel combustion route,[14,16] which makes it possible for the fabrication of quantum dot light emitting diode (QLED) devices in a convenient and cost-effective manner.

Cadmium selenide/zinc sulfide (CdSe/ZnS) QDs with core-shell structure is a popular QD material for QLED applications because their emission spectrum is within visible-wavelength and provide high brightness and high quantum efficiency.[17] For typical QLEDs, electron transport layer (ETL) and hole transport layer (HTL) are needed to facilitate the carrier transport and the radiative recombination

process. Since the first introduction of zinc oxide nanoparticles (ZnO NPs) for the ETL, it has been widely used in typical OLED and QLED devices due to its high electron injection efficiency, suitable energy bandgap and the convenience of deposition.[18,19] Compared to ZnO NPs, p-type semiconductors used as HTL materials have inferior hole injection efficiency,[20] which reduces the performance of QLEDs due to non-radiative recombination caused by unbalanced carrier injection.

To overcome the limitations of HTL materials, researchers have explored methods to further optimize the charge injection. One method for improving carrier injection is by optimizing the energy band of carrier transport layers.[20,21] Because the valence band maximum (VBM) of QDs is deep, the relatively high energy barrier between HTL and QDs layer hinders hole transportation. It has been reported in the literature that solution processed nickel oxide (NiO) is a promising transparent HTL material with a bandgap of 3.6 eV with VBM of 5.2 eV.[22,23] Moreover, it is reported that doping NiO with copper through a sol-gel method can further increase the VBM of NiO.[24,25] Thus, the energy barrier between the HTL and QDs is reduced.

In this paper, we demonstrate a novel solution processed transparent QLED device fabricated at low annealing temperatures (275 °C) that is constructed exclusively using inorganic materials. This is the first report of such a device and an important advance on the current state of the art. The all-inorganic QLEDs consists of laser-patterned tin doped indium oxide (ITO) anode, CdSe/ZnS QDs emission layer with ZnO NPs for ETL with a NiO/Cu:NiO double layer deposited before QDs, with the NiO used as a hole injection layer (HIL) with the Cu doped NiO (Cu:NiO) used as the hole transport layer. Silver nanowires (Ag NWs) were spin coated as the last step as the transparent top cathode. The complete device has a simulated transmittance of approximately 80% in the visible frequency range of 400-700 nm. By utilizing the Cu:NiO buffer layer, the turn-on voltage of the as-fabricated QLED is reduced from 4.5 V to 2.5 V, which importantly coincides with our theoretical model simulated in the COMSOL Multiphysics®.

2. Experimental Results and Discussion:

2.1 Device Structure and Fabrication Procedures

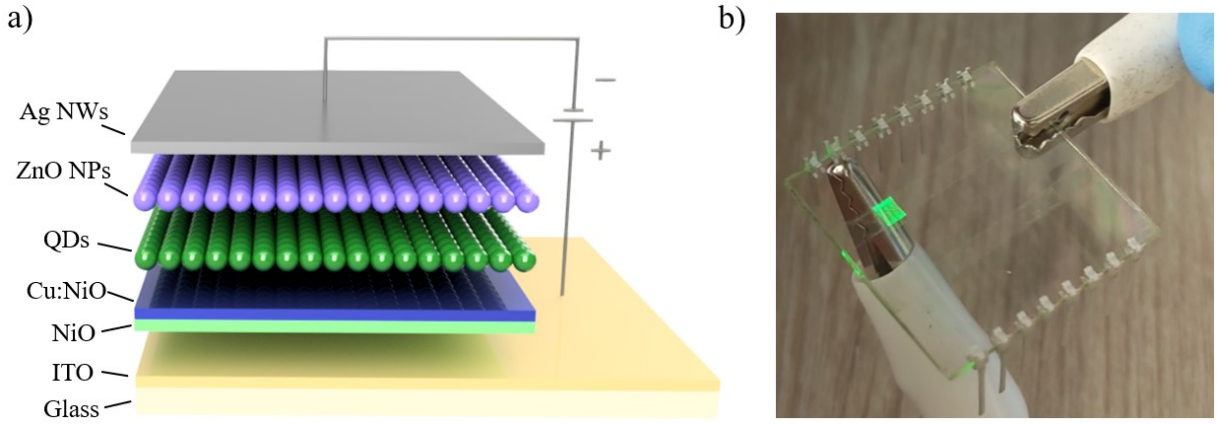

Figure 1. a) QLED structure, from bottom to top: glass substrate, ITO, NiO, Cu:NiO, QDs, ZnO NPs and Ag NWs. b) The fabricated solution processed green QLED device.

Figure 1. a) shows the device structure for solution processed QLED. It consists of ITO anode, NiO/Cu:NiO double HTLs, QDs emission layer, ZnO NPs ETL and Ag NWs cathode. The multilayered device was fabricated as shown in **Figure 1. b)**. The whole device emitting green light exhibited high optical transparency as is evidenced by the fact that the alligator clip could be seen through from the top of the device. The detailed fabrication process is illustrated in **Figure 2**. Firstly, ITO precursor was spin-coated and annealed onto the glass substrate. Laser ablation (SUSS SLP300 with solid-state laser technology at 355 nm wavelength) was used to etch the ITO film to obtain the desired patterns as QLED anodes. NiO, Cu:NiO, QDs and ZnO NPs were deposited successively on top of the previously deposited films by spin-coating, followed by annealing at each layer's specific temperature and gas environment. In the last stage, Kapton tape was used as a shadow mask and was used to spin-coat Ag NWs on top of ZnO NPs to fabricate the cathode. The electrode geometry was designed for the ease of electrical connection. Defined by the intersection of ITO and Ag NWs electrodes, the active area of a single QLED unit was 2 mm × 2 mm, which was chosen only for the convenience of probing

and measurements. The size of the QLED can be significantly reduced to produce a higher density LED pixel array.

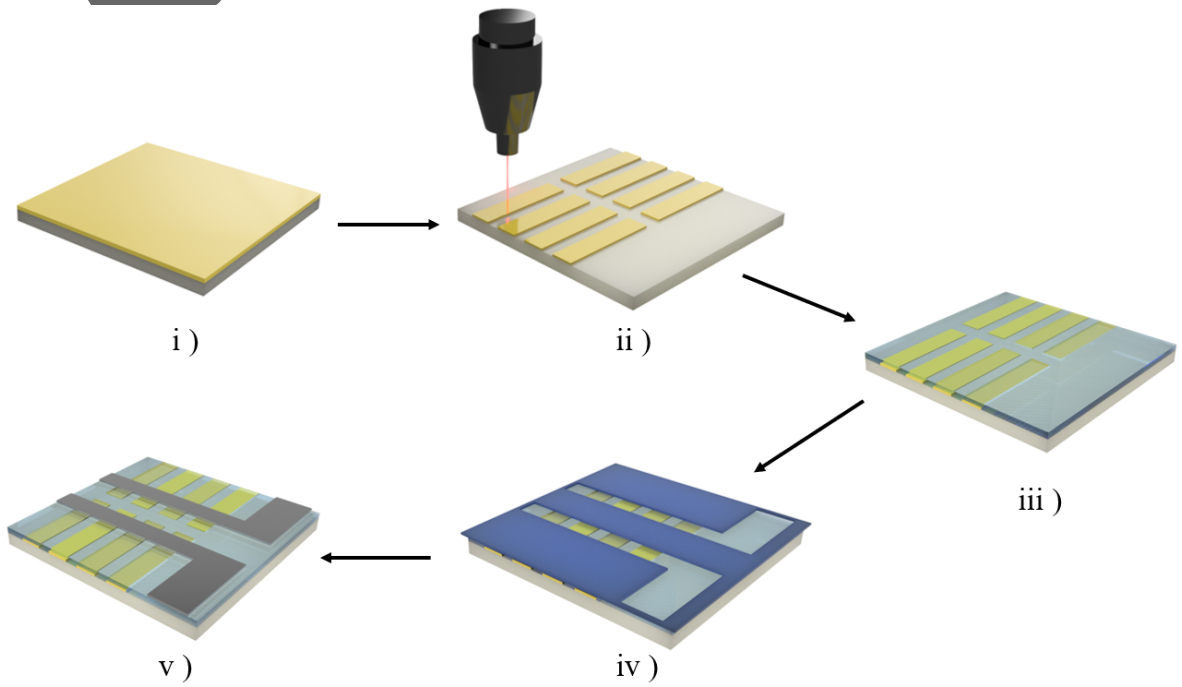

Figure 2. Fabrication procedures of QLEDs. i) spin-coat and anneal ITO on glass slide. ii) the slide is etched by laser ablation to obtain desired anode pattern. iii) spin-coat and anneal NiO, Cu:NiO, QDs and ZnO NPs layers successively. iv) attach Kapton tape as shadow mask. v) spin-coat Ag NWs followed by annealing and lift off of Kapton tape mask.

2.2 Materials Selection and Characterization

ITO is widely used as an anode electrode due to its superior conductivity and transparency. The precursor derived ITO conductivity was $10^4\ \mathrm{S\ m^{-1}}$ with a transparency above 85% in visible range.[26–28] The QDs were purchased from Mesolight Inc., having a core-shell structure of CdSe/ZnS. The photoluminescence (PL) spectrum intensity peak was located at 526 nm with full width half maximum (FWHM) wavelength being less than 30 nm, which corresponds to pure green light as shown in **Figure S1** in the supporting document. Octane was selected, instead of hexane, as the solvent because of its relatively lower volatility in comparison to hexane, resulting in a stable QDs ink. The size of the QDs was 5-10 nm and the measured quantum yield was 85%.

In concordance with the literature, for QDs to achieve maximum emission, their post-annealing temperature should always be kept below 150 °C[29] ZnO NPs were chosen to construct the ETL as a 120 °Cannealing temperature as is sufficient to remove the solvent residues from the pre-formed ZnO NPs ink, making it a perfect ETL material in this study. Similarly, the Ag NWs was selected as the cathode material due to their high transparency and low annealing temperature.[30]

The p-type NiO thin film is a promising HTL used in perovskite solar cell and LED applications[23,31–33]. It is known that p-type semiconductor materials have inferior performance over n-type semiconductor in terms of electrical conductivity and carrier mobility due to larger effective mass.[34] Doping can effectively improve the electrical properties of p-type semiconductors by changing material structure.[35] We doped NiO with Cu by adding copper nitrate into the NiO sol-gel precursor. The conductivity of annealed Cu:NiO and NiO was tested (see **Figure S3** and **Figure S4**). With Cu doping, the resistivity of the NiO film reduced from 1916 Ω·cm to 855 Ω·cm. The results are in agreement with reported resistivity measurements.[24,36]

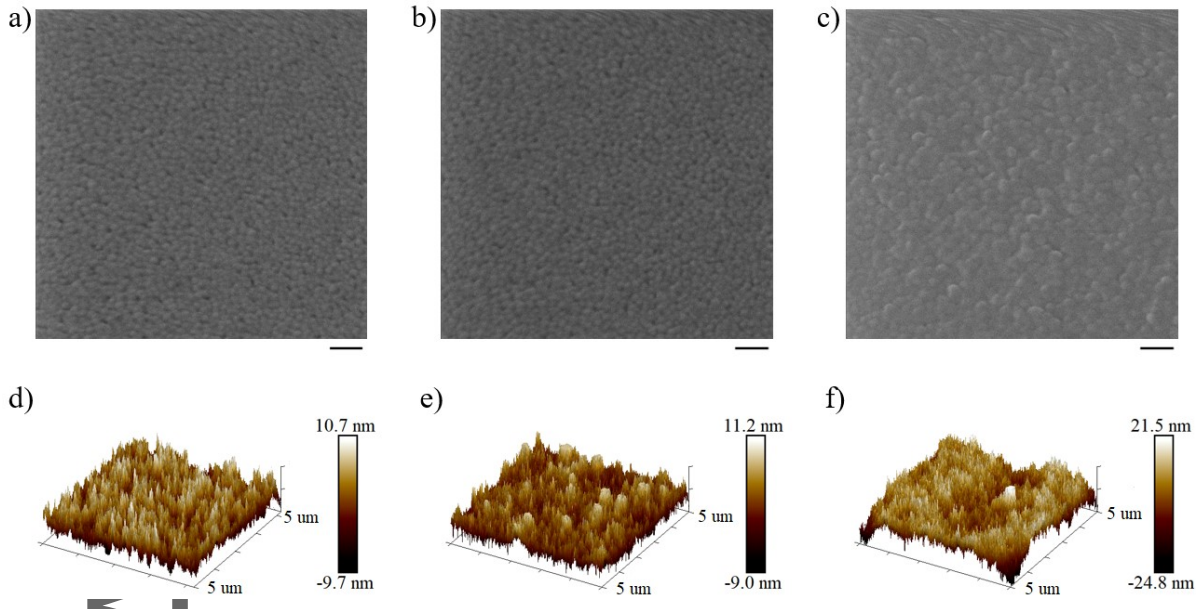

Figure 3. HIM images of a) NiO thin film annealed at 275 °C, b) Cu:NiO thin film annealed at 275 °C, and c) ZnO NPs annealed at 120 °C (Scale bar = 50 nm). AFM images of d) NiO thin film annealed at 275 °C, e) Cu:NiO thin film annealed at 275 °C, and f) ZnO NPs annealed at 120 °C

NiO and Cu:NiO were prepared via a sol-gel solution process. The thin films and ZnO NPs were spin coated on glass substrate and were imaged using helium ion microscopy (HIM). The resulting films had smooth and uniform surface morphology as is shown in **Figure 3. a) - c)**. Because the amount of Cu doping is low, there is no obvious difference between the HIM images of Cu:NiO and NiO. As a result, NiO and Cu:NiO had similar average grain size of 10.53 nm and 11.03 nm, while ZnO NPs had 17.51 nm average grain size. The grain size distribution of each film was estimated and presented in **Figure S9 - S11**. Meanwhile, atomic force microscopy (AFM) was undertaken to evaluate the surface roughness (**Figure 3 d) - f)**). The RMS roughness of NiO, Cu:NiO and ZnO NPs thin films are 3.22 nm, 3.52 nm and 5.85 nm, respectively. The relatively small RMS roughness suggests good surface morphology of the as-prepared thin films, which are in concordance with HIM results.

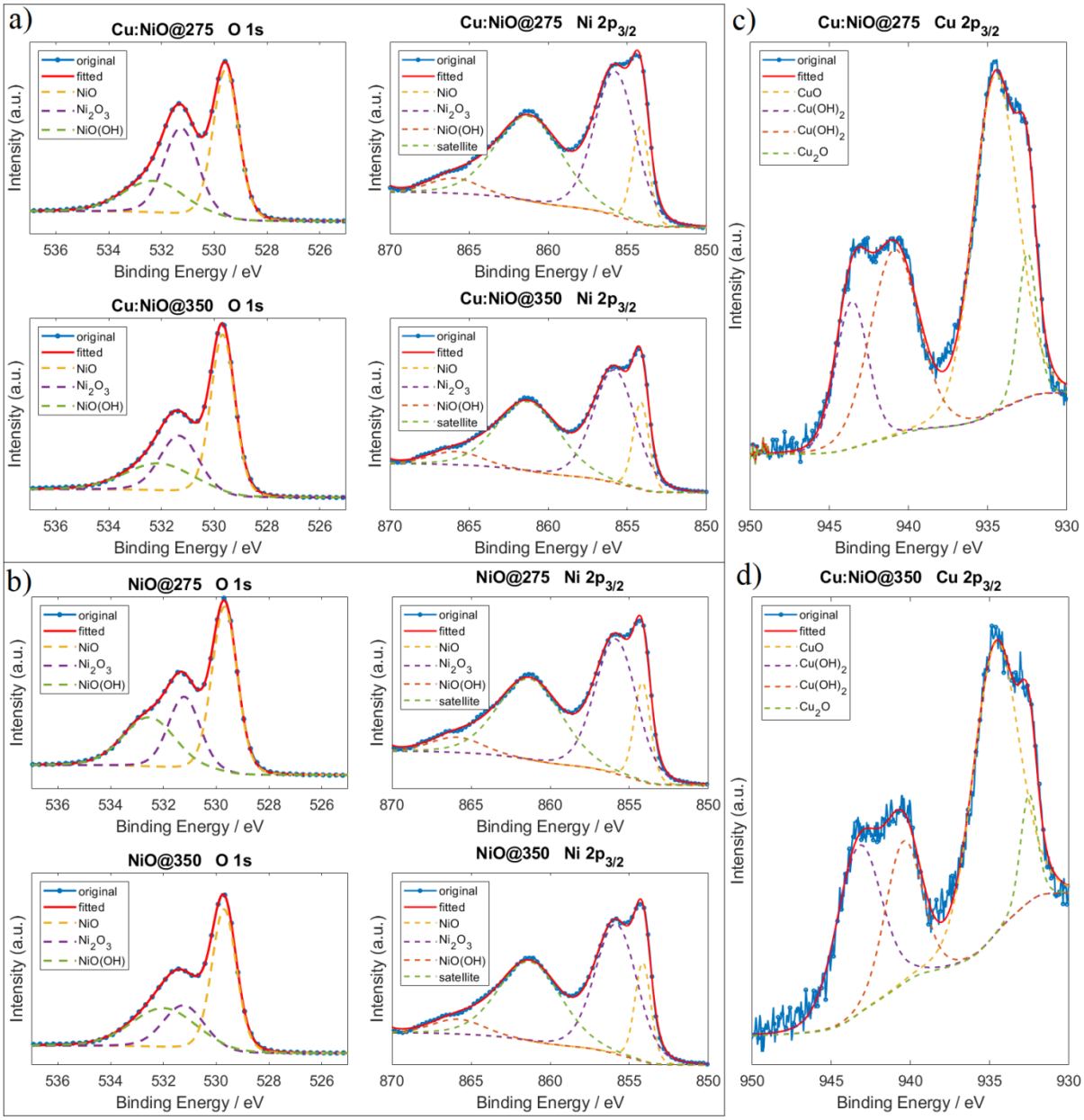

Figure 4. XPS spectra: O 1s and Ni $2p_{3/2}$ peaks of a) Cu:NiO annealed at 275 °C and 350 °C, b) NiO annealed at 275 °C and 350 °C. Cu $2p_{3/2}$ peaks of Cu:NiO c) annealed at 275 °C and d) annealed at 350 °C

In conventional sol-gel method, the NiO precursor is synthesised by dissolving nickel salts into organic solvent such as 2-methoxyethanol. After the deposition of the nickel alkoxide precursor, the substrate is heated at 350 °C to form the NiO thin film. The high annealing temperature is required to produce the meatal-oxide bond. This high annealing temperature is undesirable for QLED applications. Kim proposed a novel combustion sol-gel process to reduce the annealing temperature to as low as 200 °C by adding fuels to the sol-gel process.[16] During annealing, the fuels undertake in

an exothermic reaction, providing a local thermal source. The generated heat is absorbed and helps form the metal-oxide network even at lower external annealing temperatures.[35] We used X-ray photoemission spectroscopy (XPS) to interrogate the chemical properties of combustion derived sol-gel Cu:NiO and NiO thin film and are shown in **Figure 4**.

In **Figure 4. a)**, XPS spectra confirm the existence of Ni-O in Cu:NiO thin film. From the O 1s peaks, we can see that NiO is dominant, and the Ni is in its predominantly oxidized Ni^{2+} state. It is also worth noting that the composition of the Cu:NiO thin film did not change when annealed at higher temperature (350 °C), which supports the claim that the NiO was fully formed at 275 °C. Ni $2p_{3/2}$ peaks also prove that the Ni state did not comparatively change much when annealed at 350 °C. Furthermore, XPS results of the undoped NiO thin film are presented in **Figure 4. b)**. It shows identical O 1s and Ni $2p_{3/2}$ peaks as the spectra of Cu:NiO thin film, also indicating the formation of Ni-O bonds. In addition to Ni^{2+}, the Cu^{2+} state was also observed in the Cu $2p_{3/2}$ peaks of the spectra of Cu:NiO thin film. These are shown in **Figure 4. c)** and **Figure 4. d)**. Peaks at 933.5 eV, corresponding to Cu (II) oxide, were found in both of the Cu:NiO samples annealed at both 275 °C and 350 °C. It validates that the Cu:NiO film quality is desirable when annealed at lower temperature (275 °C), giving proof of the quality of the combustion sol-gel process.

The X-ray diffraction (XRD) measurement was performed to examine the crystallinity of Cu:NiO and NiO thin films. As shown in **Figure 5**, XRD peaks at around 36.8° and 42.8° and 62.1° were found, corresponding to the (111), (200), and (220) plane of cubic-structured NiO (JCPDS card no. 47-1049).[35] Consistent with the low Cu doping, corresponding Cu related peaks were not found which indicates that the NiO network of the thin film is not detrimentally affected. It is observed that peaks intensity of Cu:NiO is less than the peaks intensity for NiO. This can be attributed to the size of Cu^{2+} and Ni^{2+}. The ionic radius of Cu^{2+} is 0.071 nm, which is slightly larger than the ionic radius of Ni^{2+}

(0.069 nm). Thus, Cu ions may substitute Ni ions or be locate interstitial sites in the NiO lattice, causing the degradation in the crystallinity of NiO.[22]

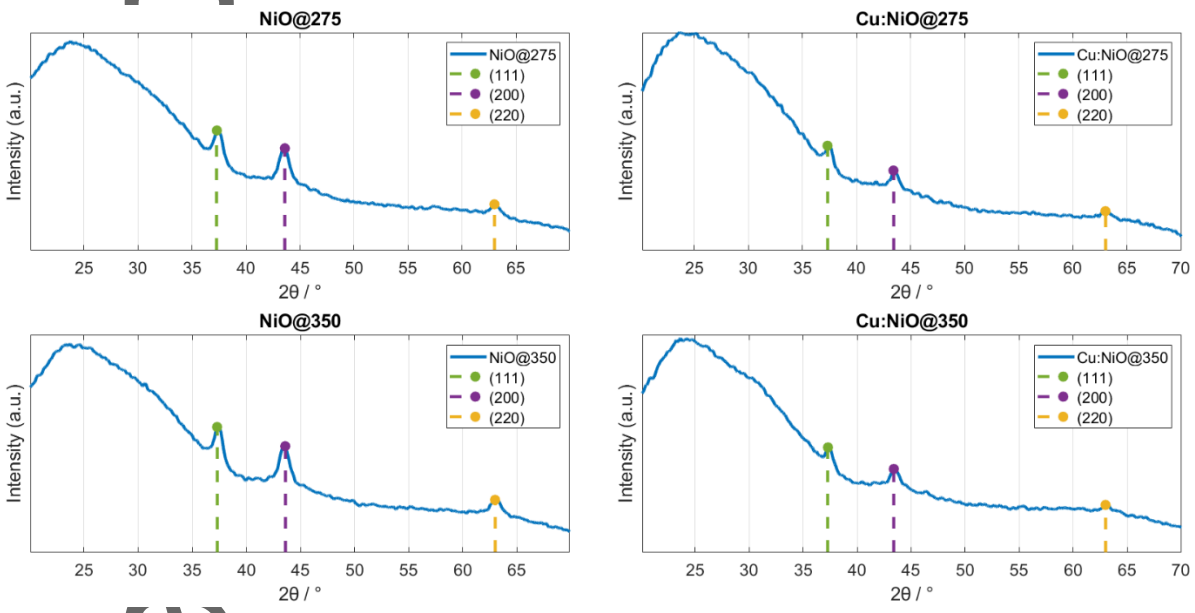

Figure 5. XRD of NiO annealed at 275 ℃ and 350 ℃, and XRD of Cu:NiO annealed at 275 ℃ and 350 ℃

2.3 Analysis of Energy Band Alignment

The energy diagrams of the materials used to construct the LED are shown in **Figure 6. a)**. To achieve low turn-on voltage QLED, energy band alignment is critical, with close alignment of VBM and conduction band minimum (CBM) between adjacent layers needed to facilitate the movement of holes and electrons for efficient radiative recombination at the QD layer.

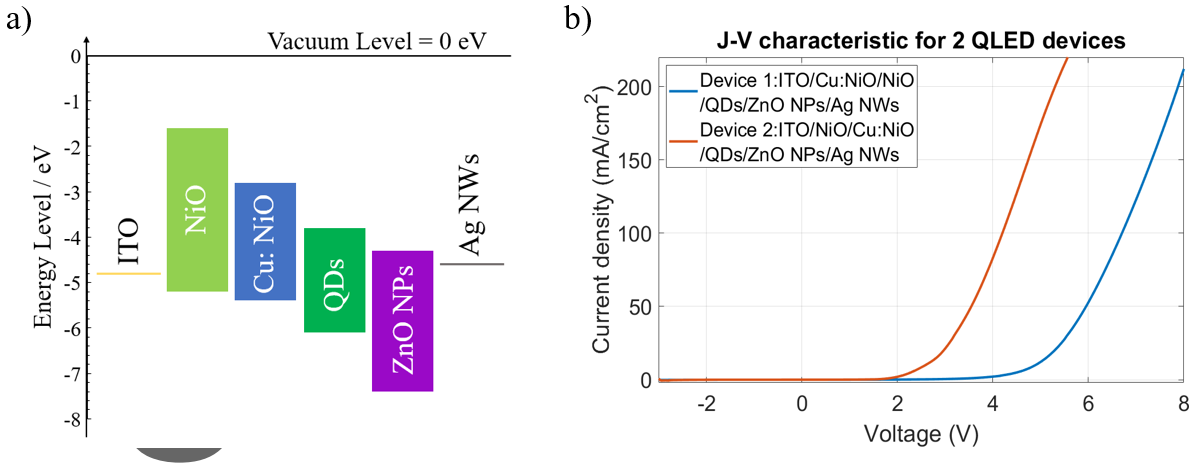

Figure 6. a) Energy band diagram of QLED device and b) J-V characteristics of QLED devices.

ZnO NPs are widely used as an electron transport layer. Since the electron transportation efficiency is higher than the hole transportation efficiency, this carrier imbalance leads to non-radiative emission called Auger recombination, which reduces the quantum efficiency.[17] To balance carrier injection, our device design strategy was to improve hole injection whilst suppressing electron injection.[20] As the VBM of QDs is around 6.2 eV, reducing the energy barrier between QDs and HTL will facilitate the transportation of holes. The VBM of NiO can be lowered with Cu doping. As shown in **Figure 6. a)**, solution processed NiO has a VBM of 5.2 eV, whereas the VBM of Cu:NiO is around 5.6 eV[23,31,37]. Therefore Cu:NiO is a suitable interlayer between NiO and QDs, providing a smoother energy band transition which minimizes the energy barrier. On the other hand, increasing the barrier height between the CBM of ZnO NPs and cathode can impede the movement of electrons. Compared to traditional Al electrode, Ag NWs have a work function of 4.6 eV, which is 0.2 eV higher than the work function of Al, resulting in a 0.3 eV difference from the CBM of ZnO NPs. This relatively larger energy difference will hinder the motion of electrons and in doing so driving the injection of both holes and electrons towards balance.

To demonstrate the importance of energy band alignment, the current density-voltage (J-V) characteristics of 2 fabricated QLEDs with different layer structures are shown in **Figure 6. b)**. It is

found that the device with Cu:NiO/NiO HTL structure shows a much higher turn-on voltage of around 4.5 V. By comparison, the device with NiO/Cu:NiO structure obtains a lower turn-on voltage of 2.5 V. This is because that the VBM of Cu:NiO is better aligned to the VBM of QDs. The Cu:NiO layer can work as a buffer layer, reducing the energy barrier between NiO and QDs. The achieved current density was 200 $\mathrm{mA\,cm^{-2}}$, which is comparable to the performance of state of art high temperature solution processed QLEDs.[37,38]

3. Simulation of QLED Using COMSOL

3.1 One-dimensional (1D) Modelling and Simulation of Electrical Properties

Simulations of QLED permits for new insights into the device operation and performance optimization. COMSOL Multiphysics is a widely used finite element analysis solver to solve real world physics problems, including semiconductor problems described by partial differential equations (PDEs). The simulated QLED structure is illustrated in **Figure 7**. It is assumed that the device is laterally invariant, having an active region with lateral dimensions of 2 mm × 2 mm. For simulation convenience, it is modelled as a one-dimensional (1D) line. It is extended to a two-dimensional (2D) QLED model for simulation of optical properties.[39] For the 1D model each line segment represents one material layer in the QLED devices. Furthermore, since the QDs have a core/shell structure, the QDs can be modelled by a sandwich structure with a CdSe core clad between ZnS shells.[40] The doping profile is shown in **Figure 8. a)**, indicating the p-type and n-type characteristics of all materials. Signed dopant concentration are displayed, where negative values correspond to net excess p-type carriers and positive values correspond to net n-type carriers.

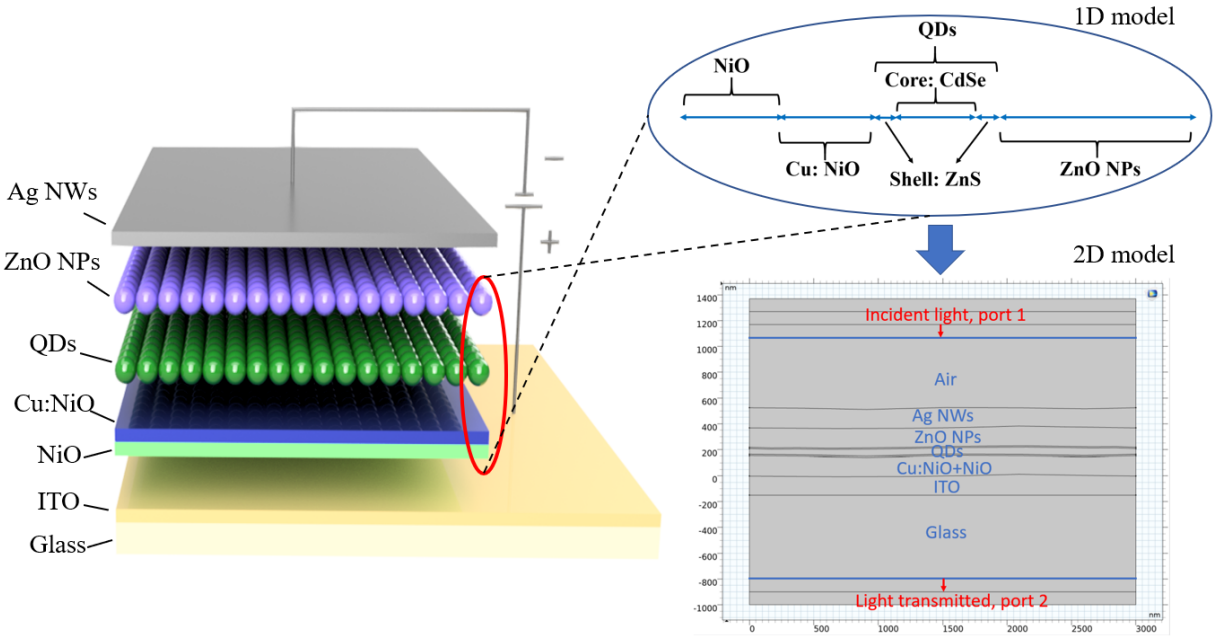

Figure 7. 1D and 2D model of QLED built in COMSOL.

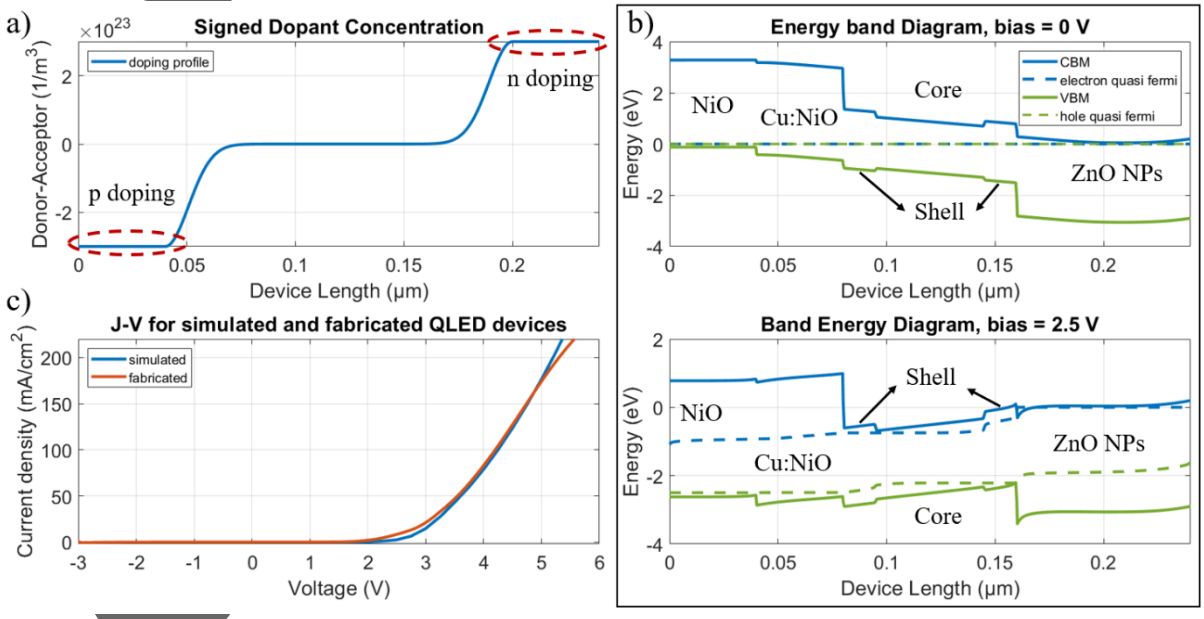

Figure 8. COMSOL simulation results. a) signed dopant concentration profile of simulated QLED; b) Energy band diagram at 0 V and 2.5 V voltage bias; c) J-V for simulated and fabricated QLED devices.

Figure 8. b) illustrates the simulated energy band diagrams of QLED. As the QDs core have surface related traps, overcoating with a shell layer helps passivate the surface defects and helps maintain colloidal stability.[17] Meanwhile, compared to QDs core, the shell layer has higher VBM and lower

CBM, which forms energy discontinuities at the boundaries, confining the electrons and holes in the core. The recombination of electrons and holes are trapped within the quantum well formed, which helps maintain the quantum efficiency. At zero voltage bias, the energy diagram is concordant with the theoretical analysis illustrated in **Figure 6. a)**. When a positive bias voltage is applied (**Figure 8. b)**), it is observed that the energy barrier is reduced, resulting in easier charge carrier transportation which facilitates the carrier recombination process. It is worth noting that the electron quasi-Fermi level and hole quasi-Fermi level are close to the edges of the conduction and valence bands, respectively. Therefore, it is expected that electrons are populated in the conduction band whilst holes are populated in the valence band. The J-V characteristics of the simulated QLED are shown in **Figure 8. c)**, along with the J-V characteristics of the fabricated QLED. By comparison, the two curves show high concordance, and identical turn-on voltage and slope.

3.1 Two-dimensional (2D) Modelling and Simulation of Optical Properties

To extract optical properties of the device, 2D QLED model has been developed. An important attribute of our QLED device is its transparency. Since the QLED has a multi-layered structure, when light with varying wavelength is incident on the interface between adjacent layers, it is reflected and transmitted in many random directions by the rough (nonuniform) interfaces. To model the randomness of the rough interface, a spatial frequencies method is introduced. Using a Fourier series expansion, the randomness of the interface curve can be modelled as a sum of trigonometric functions.[41] In the 2D model, the interface between adjacent layers is visualized as a random curve, where the height (H) of each point on the curve can be described by:[42]

$$H = h\sum_{f=-N}^{N} f^{-b} g(f)\cos(2\pi f x + u(f)) \quad (1)$$

Each frequency of oscillation of the 2D space is represented by a term in equation (1), where h is a scaling factor; f is a discrete spatial frequency; N is the number of frequency components; b is the spectral exponent indicating how quickly higher frequencies are attenuated. A Gaussian distribution

g(f) is chosen to realize the randomness of amplitude of each component, while a uniform distribution *u(f)* is used to model the variations of the phase of each component.

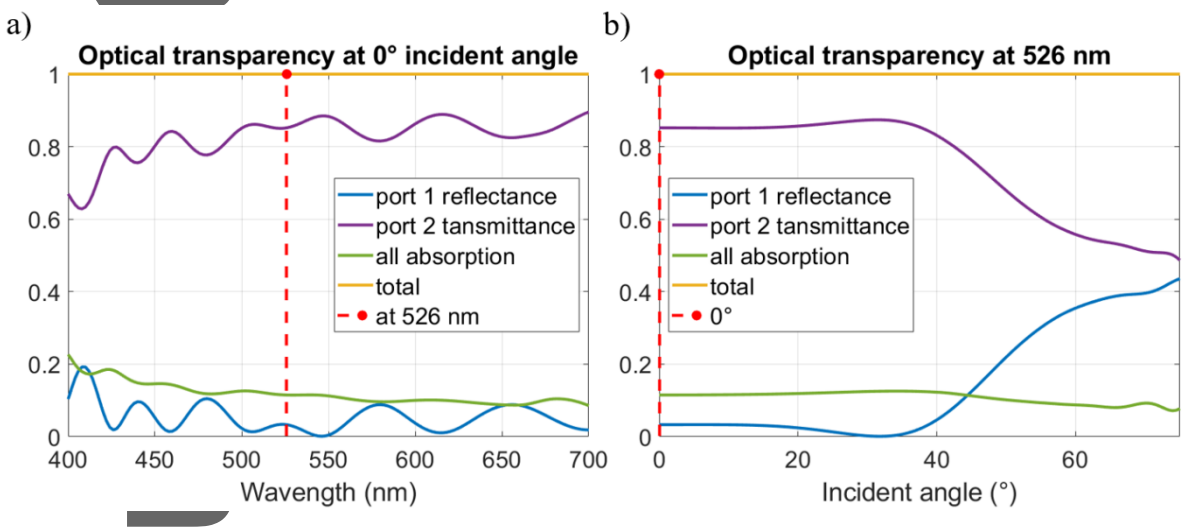

Figure 9. Transmittance, reflectance and absorption of simulated 2D QLED device. a) Wavelength sweep at 0° incident angle; b) incident angle sweep at 526 nm wavelength.

In **Figure 9**, the simulated transmittance, reflectance and absorption characteristics are shown. When the light is incident at 0° (**Figure 9. a)**), the overall transmittance of the QLED device is above 80% across the visible wavelength range. Meanwhile, simulation results accounting for angle of incidence simulation are shown in **Figure 9. b)**. When the wavelength of incident light is fixed at 526 nm (the emission wavelength of QLED), the transmittance is maintained at over 80% for incident angles less than 40° from the normal. As the incident angle continue increasing, transmittance drops. These results indicate that QLED has good visual properties when viewed perpendicular to the surface, which concords with general experience.

4. Conclusion:

In summary, we have successfully demonstrated a novel fabrication process for a solution-processed transparent inorganic QLED device. The fabrication processes are fully solution-compatible, offering a simplified way of building low-cost planar structured QLED devices and general-purpose optoelectronics. In addition, with fuel additives, the post annealing temperature was reduced to

below 275 °C, making the whole process well suited to applications requiring flexible substrates. Furthermore, this study has illustrated the importance of energy band alignment. The use of Cu:NiO buffer layer greatly reduced the QLED turn-on voltage from 4.5 V to 2.5 V, which makes the QLED compatible with CMOS electronics. In addition to experimental results, a new theoretical framework has been developed to analyse the QLED. The proposed device has been simulated and optimised in COMSOL. The simulation results show good agreement with the experimental results in terms of energy band diagram, J-V characteristics and device transparency. The combination of simulation and experiments have proven to be capable of developing new QLED design, as well as design of other optoelectronics, such as photodiode and phototransistor. We anticipate the realisation of large area, cost-effective fabrication toward high-performance transparent flexible optoelectronic applications in the near future.

5. Experimental section:

Materials and Inks preparation:

Sol-gel precursor synthesis: All reagents were purchased from Sigma Aldrich and used as received. ITO precursor ink was prepared by dissolving 54 mg $In(NO_3)_3 \cdot xH_2O$ (99.999%) and 3.78 mg $SnCl_2$ (anhydrous) in 1 mL of 2-methoxyethanol to achieve an In:Sn ratio of 9:1 with 0.2 M concentration. Then 20 µL acetylacetone (ACAC) and 14 µL NH_4OH were added into the solution as fuel and stabilizer. The molar ratio of ITO:ACAC and ITO:NH_4OH are 1:1 and 1:2, respectively. The solution was vigorously stirred at room temperature overnight.

5% molar ratio of Cu doping was selected to synthesize the Cu:NiO precursor. By dissolving 2.42 mg $Cu(NO_3)_2 \cdot 3H_2O$ (99.999%) and 55.26 mg $Ni(NO_3)_2 \cdot 6H_2O$ (99.999%) into 2 mL 2-methoxyethanol, 0.1 M Cu:NiO solution was achieved after the water-bath heating at 50 °C for 1 hour. Then 100 µL acetylacetonate was added to the solution, followed by the stirring at room temperature overnight. All precursor solutions were filtered through 0.22 µm PTFE syringe filter before use.

CdSe/ZnS quantum dots, ZnO nanoparticles were purchased from Mesolight Inc. The quantum dots are dissolved in Octane to reach a concentration of 10 mg mL^{-1}. For ZnO nanoparticles, the concentration is 20 mg mL^{-1} in ethanol solvent. TranDuctive N30 Ag NWs ink was purchased from GenesInk.

QLED Fabrication: The QLED devices were built on 25 mm × 25 mm 1.1 mm thick glass slides. Firstly, the slides were cleaned by successive ultrasonication in Acetone, IPA and water for 8 mins, respectively. Then the slides were treated by O_2 plasma for 10 mins with 50 W Rf power.

To achieve a good layer condition, each layer requires spin-coating and annealing three times. ITO precursor was spin-coated on the cleaned slides at 3000 rpm for 40 s, followed by 350 °C annealing in

N_2 for 1 hour. Then the ITO was etched by SUSS SLP300 laser ablation machine, using 355 nm laser beam to generate desired anode pattern. Before the next spin-coating process, the ITO slides were cleaned and treated by O_2 plasma for 10 mins with 50 W Rf power to improve the hydrophilicity. Next, the NiO and Cu:NiO precursor were deposited onto the ITO coated slides by spin-coating at 3000 rpm for 40 s, followed by 1-hour annealing at 275 °C in air, respectively. Similarly, the Cu:NiO films required O_2 plasma treatment for better interfacing. After this, the slides were spin-coated by QDs ink at 3000 rpm for 40 s. Samples were then placed on hotplate and annealed in N_2 at 120 °C for 20 mins. ZnO NPs were deposited in the same way as QDs. At last, Ag NWs cathodes were spin-coated at 2000 rpm and annealed at 100 °C for 10 mins. The cathode pattern was defined by Kapton tape shadow mask.

The stability of the QLED is enhanced because of the use of inorganic materials. Encapsulation has also been investigated to improve the QLED lifetime. Ossila E132 Encapsulation Epoxy was applied to cover the device, after which time a glass coverslip was placed over the top of the device. After the epoxy spread uniformly, the device was cured under UV light for 1 min. The device lifetime can be extended to over 10 days.

Characterization: The high magnification electron microscope images were obtained by helium ion microscope, Orion Nanofab, Carl Zeiss. AFM measurements were undertaken by Bruker's Dimension Icon, while XRD measurements are made by Bruker D8. XPS measurements were performed on Kratos Axis Supra XPS. In order to prepare the XPS and XRD samples, thin film materials were spin coated on 1×1 cm^2 glass slides for characterization. The sheet resistivity and J-V characteristic of sol-gel derived thin film and QLED were measured by four-probe measurement using Cascade Microtech Summit semi-automated Probe Station with Agilent E5270B Precision IV Analyser.

Supporting Information

Please see the supporting document provided.

Acknowledgements

This work would not have been possible without ANFF facilities. ANFF facilities where used in all facets of this research beginning from access to simulation software to device fabrication using facilities and lithography equipment at the ANFF. Lithography was used to produce shadow masks used in these devices. Thin Film characterisation and thickness were also undertaken at ANFF facilities. Device Imaging was performed using microscopy equipment and facilities made available through the ANFF.

References

[1] S. Kim, S. W. Hwang, M. Kim, D. Y. Shin, D. H. Shin, C. O. Kim, K. I. M. E. T. Al, **2012**, 8203.

[2] O. Salihoglu, N. Kakenov, O. Balci, S. Balci, C. Kocabas, *ACS Photonics* **2018**, *5*, 2384.

[3] Q. Sun, Y. A. Wang, L. S. Li, D. Wang, T. Zhu, J. Xu, C. Yang, Y. Li, *Nat. Photonics* **2007**, *1*, 717.

[4] T. H. Kim, K. S. Cho, E. K. Lee, S. J. Lee, J. Chae, J. W. Kim, D. H. Kim, J. Y. Kwon, G. Amaratunga, S. Y. Lee, B. L. Choi, Y. Kuk, J. M. Kim, K. Kim, *Nat. Photonics* **2011**, *5*, 176.

[5] J. M. Caruge, J. E. Halpert, V. Wood, V. Buloví, M. G. Bawendi, *Nat. Photonics* **2008**, *2*, 247.

[6] K. S. Cho, E. K. Lee, W. J. Joo, E. Jang, T. H. Kim, S. J. Lee, S. J. Kwon, J. Y. Han, B. K. Kim, B. L. Choi, J. M. Kim, *Nat. Photonics* **2009**, *3*, 341.

[7] H. Chen, Y. Cao, J. Zhang, C. Zhou, *Nat. Commun.* **2014**, *5*, 1.

[8] S. K. Garlapati, T. T. Baby, S. Dehm, M. Hammad, V. S. K. Chakravadhanula, R. Kruk, H. Hahn, S. Dasgupta, *Small* **2015**, *11*, 3591.

[9] N. Cui, H. Ren, Q. Tang, X. Zhao, Y. Tong, W. Hu, Y. Liu, *Nanoscale* **2018**, *10*, 3613.

[10] J. Yong, Y. Liang, Y. Yu, B. Hassan, M. S. Hossain, K. Ganesan, R. R. Unnithan, R. Evans, G. Egan, G. Chana, B. Nasr, E. Skafidas, *ACS Appl. Mater. Interfaces* **2019**, *11*, 17521.

[11] P. Yang, L. Zhang, D. J. Kang, R. Strahl, T. Kraus, *Adv. Opt. Mater.* **2020**, *8*, 1.

[12] C. Xiang, L. Wu, Z. Lu, M. Li, Y. Wen, Y. Yang, W. Liu, T. Zhang, W. Cao, S. W. Tsang, B. Shan, X. Yan, L. Qian, *Nat. Commun.* **2020**, *11*, 1.

[13] M. Kurihara, **2014**, *16*.

[14] K. K. Banger, Y. Yamashita, K. Mori, R. L. Peterson, T. Leedham, J. Rickard, H. Sirringhaus, *Nat. Mater.* **2011**, *10*, 45.

[15] Y. H. Kim, J. S. Heo, T. H. Kim, S. Park, M. H. Yoon, J. Kim, M. S. Oh, G. R. Yi, Y. Y. Noh, S. K. Park, *Nature* **2012**, *489*, 128.

[16] M. G. Kim, M. G. Kanatzidis, A. Facchetti, T. J. Marks, *Nat. Mater.* **2011**, *10*, 382.

[17] Y. Shirasaki, G. J. Supran, M. G. Bawendi, V. Bulović, *Nat. Photonics* **2013**, *7*, 13.

[18] L. Qian, Y. Zheng, J. Xue, P. H. Holloway, *Nat. Photonics* **2011**, *5*, 543.

[19] B. S. Mashford, M. Stevenson, Z. Popovic, C. Hamilton, Z. Zhou, C. Breen, J. Steckel, V. Bulovic, M. Bawendi, S. Coe-Sullivan, P. T. Kazlas, *Nat. Photonics* **2013**, *7*, 407.

[20] Y. Sun, Y. Jiang, H. Peng, J. Wei, S. Zhang, S. Chen, *Nanoscale* **2017**, *9*, 8962.

[21] Y. Liu, C. Jiang, C. Song, J. Wang, L. Mu, Z. He, Z. Zhong, Y. Cun, C. Mai, J. Wang, J. Peng, Y. Cao, *ACS Nano* **2018**, *12*, 1564.

[22] Y. E. Firat, A. Peksoz, *Electrochim. Acta* **2018**, *295*, 645.

[23] D. Saranin, P. Gostischev, D. Tatarinov, I. Ermanova, V. Mazov, D. Muratov, A. Tameev, D. Kuznetsov, S. Didenko, A. Di Carlo, *Materials (Basel).* **2019**, *12*, 1406.

[24] J. W. Jung, C. C. Chueh, A. K. Y. Jen, *Adv. Mater.* **2015**, *27*, 7874.

[25] K. H. Kim, C. Takahashi, Y. Abe, M. Kawamura, *Optik (Stuttg).* **2014**, *125*, 2899.

[26] Z. Chen, W. Li, R. Li, Y. Zhang, G. Xu, H. Cheng, *Langmuir* **2013**, *29*, 13836.

[27] Y. Liang, J. Yong, Y. Yu, A. Nirmalathas, K. Ganesan, R. Evans, B. Nasr, E. Ska, **2019**.

[28] B. Hassan, Y. Liang, J. Yong, Y. Yu, K. Ganesan, A. Walla, R. Evans, G. Chana, B. Nasr, E. Skafidas, *Flex. Print. Electron.* **2018**, *3*.

[29] B. S. Mashford, T. L. Nguyen, G. J. Wilson, P. Mulvaney, *J. Mater. Chem.* **2010**, *20*, 167.

[30] A. B. V. K. Kumar, J. Jiang, C. W. Bae, D. M. Seo, L. Piao, S. H. Kim, *Mater. Res. Bull.* **2014**, *57*,

52.

[31] J. Kim, H. R. Lee, H. P. Kim, T. Lin, A. Kanwat, A. R. Bin Mohd Yusoff, J. Jang, *Nanoscale* **2016**, *8*, 9284.

[32] J. H. Kim, P. W. Liang, S. T. Williams, N. Cho, C. C. Chueh, M. S. Glaz, D. S. Ginger, A. K. Y. Jen, *Adv. Mater.* **2015**, *27*, 695.

[33] J. You, L. Meng, T. Bin Song, T. F. Guo, W. H. Chang, Z. Hong, H. Chen, H. Zhou, Q. Chen, Y. Liu, N. De Marco, Y. Yang, *Nat. Nanotechnol.* **2016**, *11*, 75.

[34] J. Yu, G. Liu, A. Liu, Y. Meng, B. Shin, F. Shan, *J. Mater. Chem. C* **2015**, *3*, 9509.

[35] A. Liu, H. Zhu, Z. Guo, Y. Meng, G. Liu, E. Fortunato, R. Martins, F. Shan, *Adv. Mater.* **2017**, *29*, 1.

[36] Y. H. Li, X. Lu, R. Wang, Y. Y. Ma, S. Duhm, M. K. Fung, *J. Mater. Chem. C* **2017**, *5*, 11751.

[37] F. Cao, H. Wang, P. Shen, X. Li, Y. Zheng, Y. Shang, J. Zhang, Z. Ning, X. Yang, *Adv. Funct. Mater.* **2017**, *27*, 1.

[38] H. Zhang, X. Sun, S. Chen, **2017**, *1700610*, 1.

[39] COMSOL, *InGaN / AlGaN Double Heterostructure LED*, **2014**.

[40] M. K. Choi, J. Yang, D. C. Kim, Z. Dai, J. Kim, H. Seung, V. S. Kale, S. J. Sung, C. R. Park, N. Lu, T. Hyeon, D. Kim, **2018**, *1703279*, 1.

[41] W. Frei, *How to Model the Optical Properties of Rough Surfaces*, **2017**.

[42] B. Sjödin, *How to generate random surfaces in Comsol Multiphysics*, Vol. 2017, **2017**.

Table of Contents

Simulation and Fabrication of Low Temperature Solution Processed Transparent QLED Using Inorganic Metal Oxide Carrier Transport Layers

Yang Yu, You Liang, Jason Yong, TianZhi Li, Md Sharafat Hossain, Yutong Liu, Yihong Hu, Kumaravelu Ganesan, Efstratios Skafidas**

In this paper, a transparent solution processed inorganic QLED device is fabricated. The low-temperature sol-gel derived copper doped nickel oxide interlayer improves the hole injection efficiency, reducing the QLED turn-on voltage. Meanwhile, the modelling and simulation of QLED are completed in COMSOL, where the simulation results showed good accordance with the experimental results and theoretical analysis.

(50-60 words)

ToC figure: 55 mm by 50 mm